

Evidence for a hopping mechanism in metal | single molecule | metal junctions involving conjugated metal–terpyridyl complexes; potential-dependent conductances of complexes $[M(\text{pyterpy})_2]^{2+}$ (M = Co and Fe; pyterpy = 4'-(pyridin-4-yl)-2,2':6',2''-terpyridine) in ionic liquid.

Sarah Chappell¹, Carly Brooke¹, Richard J. Nichols¹, Laurence J. Kershaw Cook,² Malcolm Halcrow,² Jens Ulstrup³ and Simon J. Higgins^{1*}

Supplementary information

Contents

| | | |
|----|---|----|
| 1. | Additional synthetic details | 2 |
| 2. | Data acquisition and processing for the metal molecule metal conductance experiments. | |
| | 2.1 <i>Experimental details</i> | 6 |
| | 2.2 <i>I(s) data acquisition and data selection</i> | 6 |
| | 2.3 <i>Break-off distance estimation</i> | 7 |
| 3. | Additional <i>I(s)</i> data. | |
| | 3.1 <i>Data sets on pyterpy complexes</i> | 7 |
| | 3.2 <i>Length dependence of conductance experiments, recorded in ambient.</i> | 9 |
| | 3.3 <i>I(s) data from potential-dependence of conductance determinations.</i> | 11 |
| 4. | Additional references | 11 |

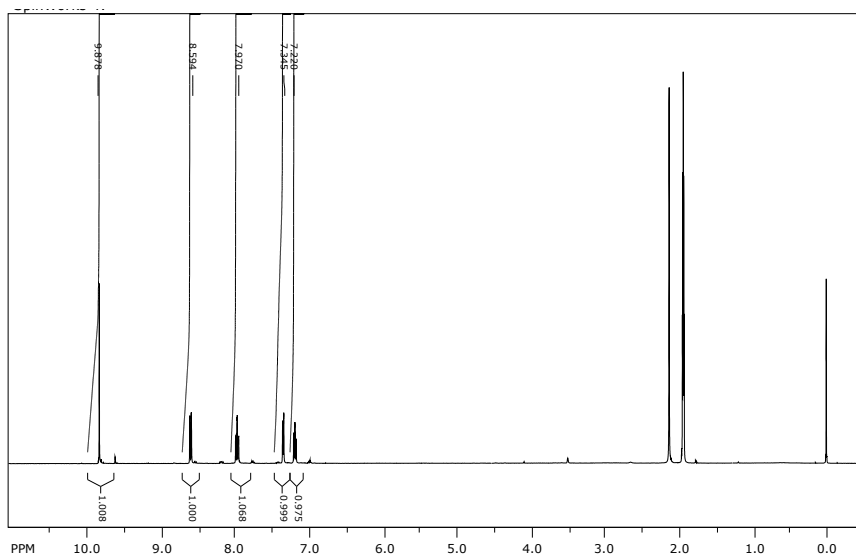


Figure S2 ^1H NMR spectrum of $[\text{Ru}(\text{dipy-pyraz})_2](\text{PF}_6)_2$ in CD_3CN .

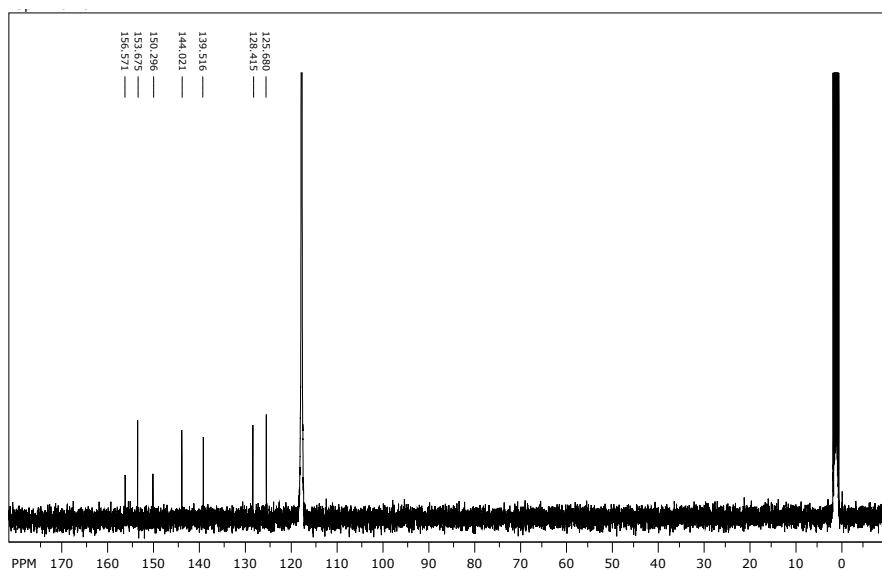


Figure S3 $^{13}\text{C}\{^1\text{H}\}$ NMR spectrum of $[\text{Ru}(\text{dipy-pyraz})_2](\text{PF}_6)_2$ in CD_3CN .

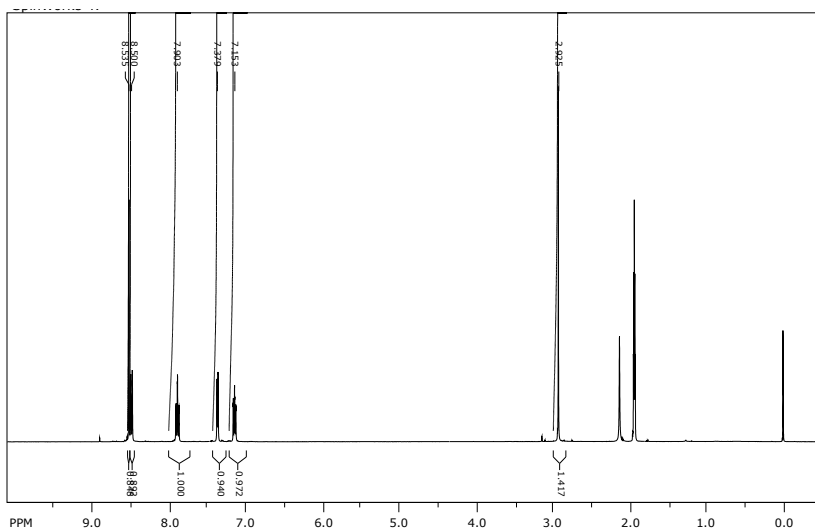


Figure S4 ^1H NMR spectrum of $[\text{Ru}(\text{MeSterpy})_2](\text{PF}_6)_2$ in CD_3CN .

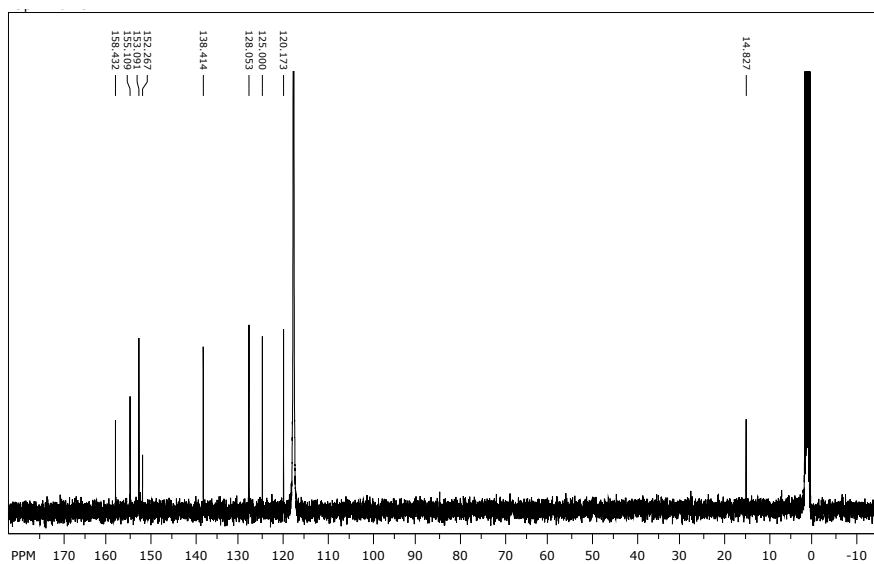


Figure S5 $^{13}\text{C}\{^1\text{H}\}$ NMR spectrum of $[\text{Ru}(\text{MeSterpy})_2](\text{PF}_6)_2$ in CD_3CN .

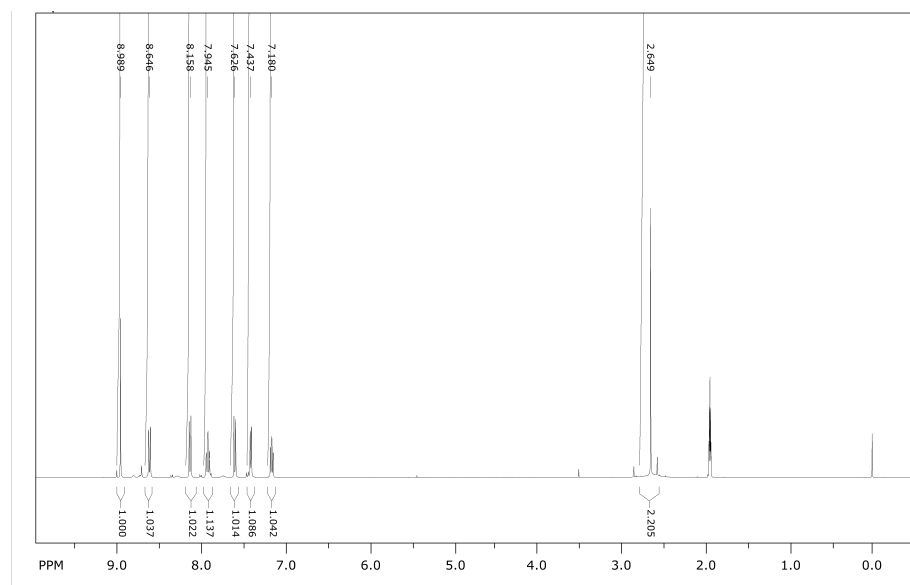


Figure S6 ^1H NMR spectrum of $[\text{Ru}(\text{MeS-ph-terpy})_2](\text{PF}_6)_2$ in CD_3CN .

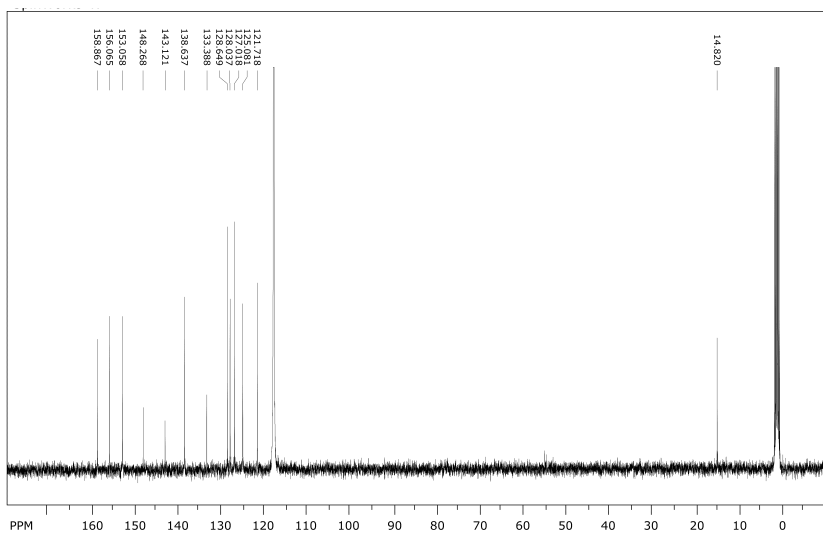


Figure S7 $^{13}\text{C}\{^1\text{H}\}$ NMR spectrum of $[\text{Ru}(\text{MeS-ph-terpy})_2](\text{PF}_6)_2$ in CD_3CN .

2. Data acquisition and processing for the metal | molecule | metal conductance experiments.

2.1 Experimental details

Measurements were made using an Agilent 2500 or 5500 controller utilizing Agilent PicoScan 5.3.3 software. Gold on glass substrates (Arrandee®) were flame annealed prior to use by gentle heating with a butane torch for approximately 2 minutes, a procedure known to produce Au(111) terraces.¹ Gold tips were prepared by cutting 0.25 mm gold wire (99.99%, Goodfellows). The BMIM TFSI ionic liquid was dried before use by heating to 100 °C under vacuum overnight.

Low-coverage monolayers were formed by immersing the flame-annealed gold substrates into dilute solutions (typically 5×10^{-5} M) of the required molecule in CH_2Cl_2 for a set time, typically 1-2 minutes. The substrate was then washed with CH_2Cl_2 then ethanol, and dried with a nitrogen stream before being mounted in the STM. For conductance measurements denoted as recorded in ambient, the measurements were made in the laboratory atmosphere, with no liquid environment. For measurements in ionic liquid, an environmental chamber was used with a dry nitrogen atmosphere, and for measurements under electrochemical control, Pt quasi-reference and counter electrodes were employed, with the ferrocene/ferrocenium redox couple used as a reference. Once the ionic liquid was added to the cell, the system was purged with nitrogen for 1 h prior to use.

2.2 $I(s)$ data acquisition and data selection

Data acquisition and selection was performed using methods that are currently routine in our group.² Single molecule conductance $I(s)$ measurements^{3,4} were made using an Agilent 5500 STM controller in conjunction with Agilent Picoscan 5.3.3 software. The tip was held at a constant xy position over a Au(111) terrace previously located using scanning, and was brought to an initial height (s_0) using a fixed setpoint current (I_0) of 40 nA (20 nA for the two longest molecules, as noted in the paper) and a bias voltage (V_{bias}) of + 0.6 V. The tip was then withdrawn 4 nm relative to the setpoint with the feedback loop disabled to enable tunneling current to be monitored; the scan duration was 0.1 s. The feedback loop was then re-engaged and the tip was brought back to s_0 . All current–distance (i - s) traces containing a plateau or plateaus longer than 0.1 nm were used in the histogram analyses; traces that were simply noisy, or that showed only an exponential decay of i with s , were not used.

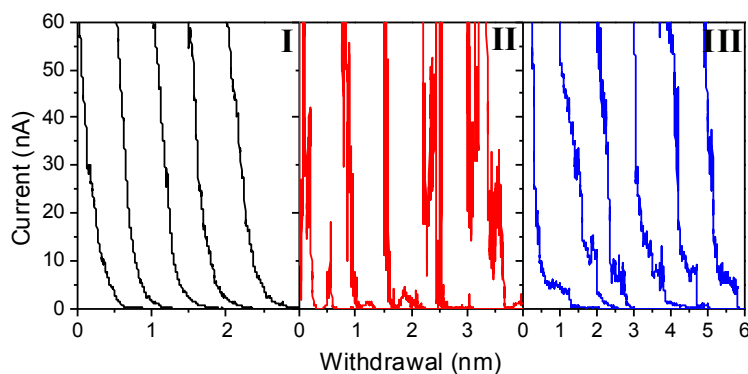


Figure S8. Typical $I(s)$ traces observed during tip-withdrawal experiments. (I) Examples of i - s traces showing smooth exponential decay (typically, ca. 70 % of traces for experiments with pyridyl-contacted molecules). (II)

Examples of i - s traces showing non-monotonic and noisy characteristics (typically, ca. 20 % of traces for the experiments in this study). (III) Examples of i - s traces showing step-like features as the tip is withdrawn.

2.3 Break-off distance estimation

To further confirm the formation of molecular junctions an estimated break off distance (s_{total}) was calculated and compared to the length of the molecule when trapped between two gold atoms (calculated using Spartan®). The total break off distance s_{total} is a sum of two components; $s_{total} = s_0 + \Delta s$ where Δs is the distance at which the current plateau ends and s_0 is the height of the tip above the gold surface at the start of the experiment. The latter was estimated by a literature procedure. Briefly, several of the I - s scans that resulted in only exponential decay are plotted as $\ln(I)$ versus s in the distance range relevant to the experiment. Linear regression was then used to determine $d(\ln I)/d(s)$. The distance between the tip and substrate was then calculated at a given set point value (I_0) using:

$$s_0 = s_0 = \frac{\ln\left(G_0 \cdot \frac{V_{bias}}{I_0}\right)}{d(\ln I)/d(s)}$$

Where G_0 is the point contact conductance of gold (77500 nS) and V_{bias} is the bias applied. Δs was calculated for every plateau included in the conductance histogram and often showed some variation due to the random nature of the junction breaking process. For each data set, around 500 scans with plateaus meeting the above criteria were collected and the data were plotted into a histogram to calculate the conductance. The uncertainties quoted are the peak widths at half height. The ‘hit rate’ referred to in the paper is the ratio of I - s scans with plateaus to those (either noisy, or with simple exponential current decay) without.

3. Additional $I(s)$ data

3.1 Data sets on pyterpy complexes, recorded in ambient conditions unless otherwise noted.

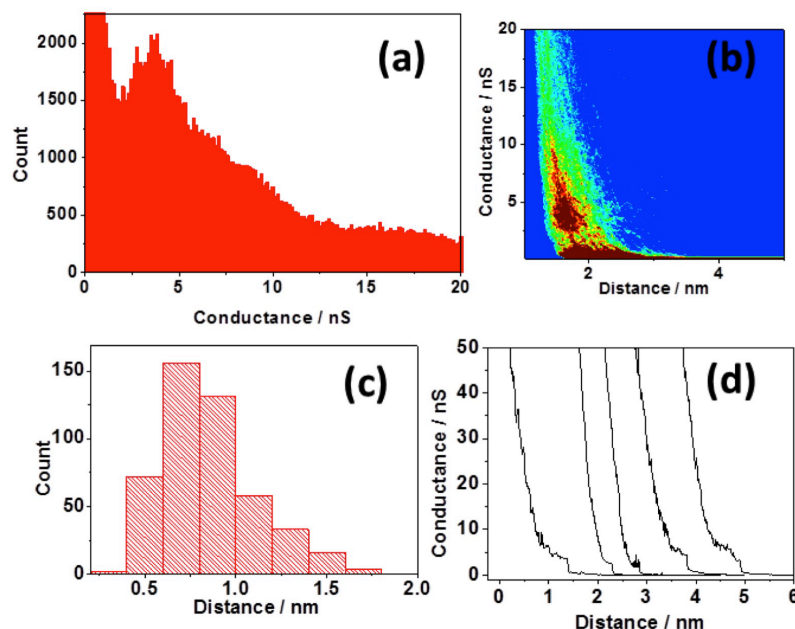


Figure S9. $I(s)$ data recorded for $[\text{Ru}(\text{pyterpy})_2](\text{PF}_6)_2$, $I_0 = 40$ nA, $V_{bias} = 0.6$ V: (a) One-dimensional histogram of the 520 I - s traces collected that showed plateau(x), (b) two-dimensional representation of conductance vs corrected break-off distance for all plateau(s)-containing traces, (c) histogram of uncorrected break-off distances for all plateau(x)-containing traces, (d) some representative plateau(s)-containing I - s traces.

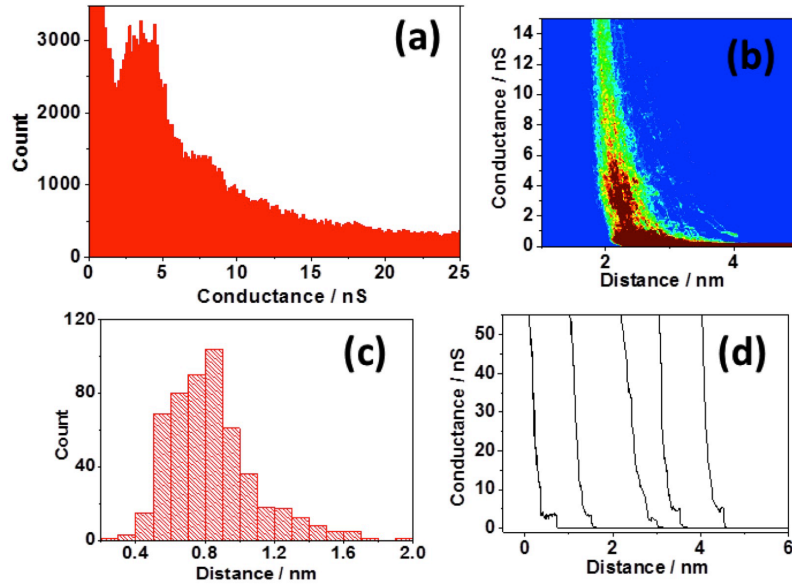


Figure S10. $I(s)$ data recorded for $[\text{Co}(\text{pyterpy})_2](\text{PF}_6)_2$, $I_0 = 40 \text{ nA}$, $V_{\text{bias}} = 0.6 \text{ V}$: (a) One-dimensional histogram of the 508 I - s traces collected that showed plateau(s), (b) two-dimensional representation of conductance vs corrected break-off distance for all plateau(s)-containing traces, (c) histogram of uncorrected break-off distances for all plateau(s)-containing traces, (d) some representative plateau(s)-containing I - s traces.

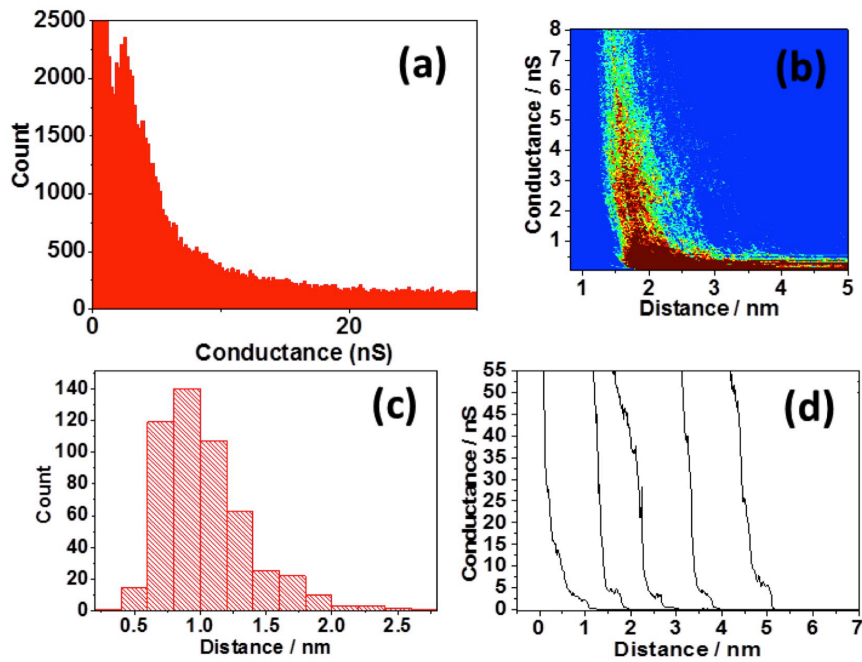


Figure S11. $I(s)$ data recorded for $[\text{Cr}(\text{pyterpy})_2](\text{PF}_6)_3$, $I_0 = 40 \text{ nA}$, $V_{\text{bias}} = 0.6 \text{ V}$: (a) One-dimensional histogram of the 511 I - s traces collected that showed plateau(s), (b) two-dimensional representation of conductance vs corrected break-off distance for all plateau(s)-containing traces, (c) histogram of uncorrected break-off distances for all plateau(s)-containing traces, (d) some representative plateau(s)-containing I - s traces.

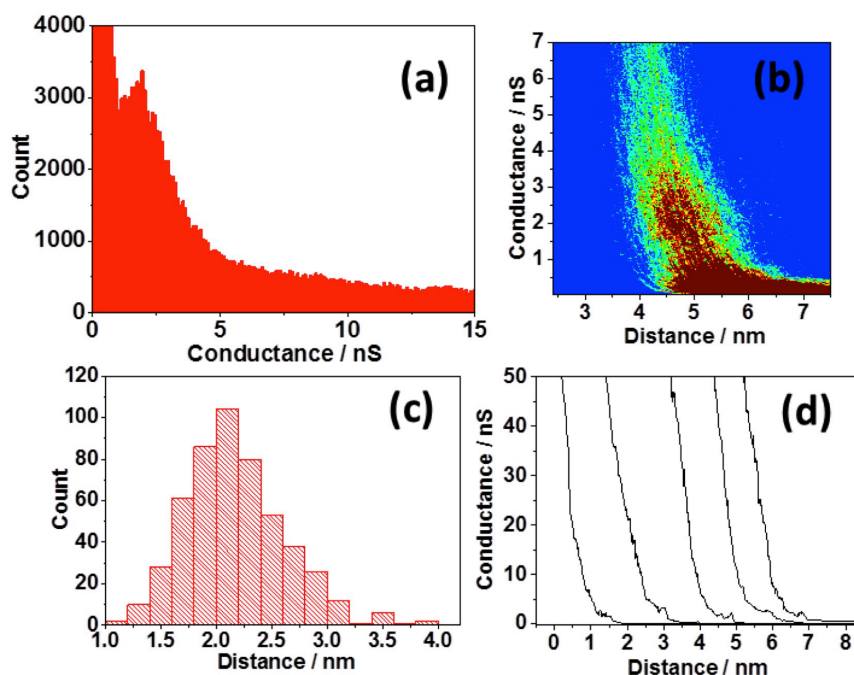


Figure S12. $I(s)$ data recorded for $[\text{Cr}(\text{pyterpy})_2](\text{PF}_6)_3$ in BMIM TFSI ionic liquid under nitrogen (but not under potential control), $I_0 = 40$ nA, $V_{\text{bias}} = 0.6$ V: (a) One-dimensional histogram of the 510 $I-s$ traces collected that showed plateau(s), (b) two-dimensional representation of conductance vs corrected break-off distance for all plateau(s)-containing traces, (c) histogram of uncorrected break-off distances for all plateau(s)-containing traces, (d) some representative plateau(s)-containing $I-s$ traces. The calculated conductance for this experiment was 2.0 ± 0.3 nS ($(2.6 \pm 0.4) \times 10^{-5} G_0$), identical to the value measured in ambient within experimental uncertainty, showing that there is insignificant dependence of the conductance on the medium (air, or ionic liquid) in these complexes.

3.2 Length dependence of conductance experiments, recorded in ambient.

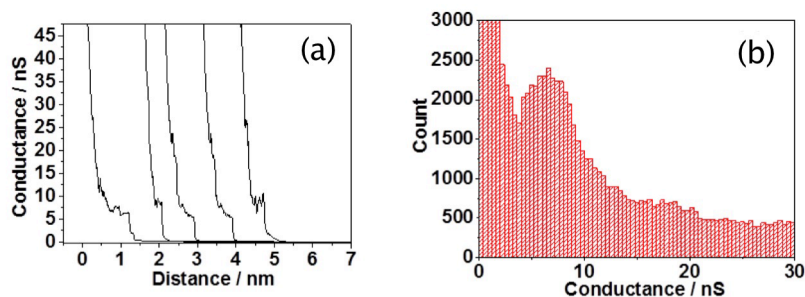


Figure S13. $I(s)$ data recorded for $[\text{Ru}(\text{dipy-pyraz})_2](\text{PF}_6)_2$, $I_0 = 40$ nA, $V_{\text{bias}} = 0.6$ V: (a) Some representative plateau(s)-containing $I-s$ traces, (b) one-dimensional histogram of the 506 $I-s$ traces collected that showed plateau(s).

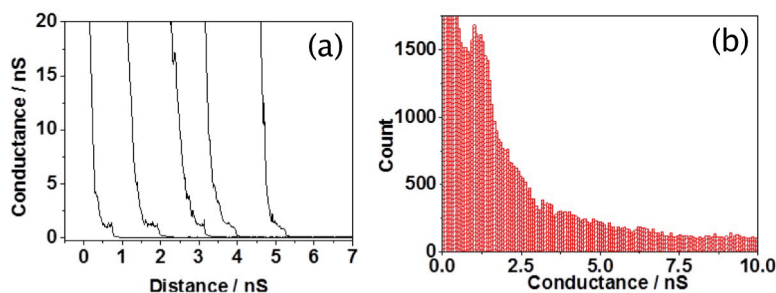


Figure S14. $I(s)$ data recorded for $[\text{Ru}(\text{py-ph-ph-terpy})_2](\text{PF}_6)_2$, $I_0 = 20$ nA, $V_{\text{bias}} = 0.6$ V: (a) Some representative plateau(s)-containing $I-s$ traces, (b) one-dimensional histogram of the 468 $I-s$ traces collected that showed plateau(s).

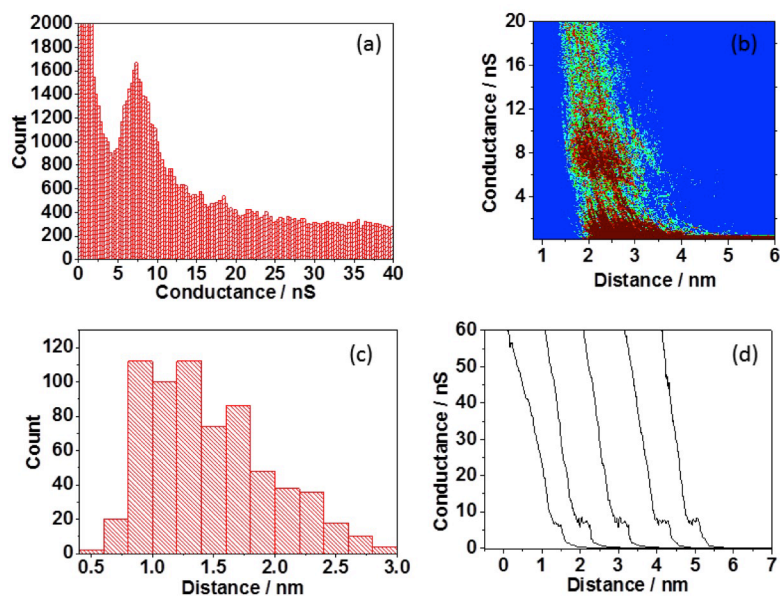


Figure S15. $I(s)$ data recorded for $[\text{Ru}(\text{MeSterpy})_2](\text{PF}_6)_2$, $I_0 = 40 \text{ nA}$, $V_{\text{bias}} = 0.6 \text{ V}$: (a) One-dimensional histogram of the 542 I - s traces collected that showed plateau(s), (b) two-dimensional representation of conductance vs corrected break-off distance for all plateau(s)-containing traces, (c) histogram of uncorrected break-off distances for all plateau(s)-containing traces, (d) some representative plateau(s)-containing I - s traces.

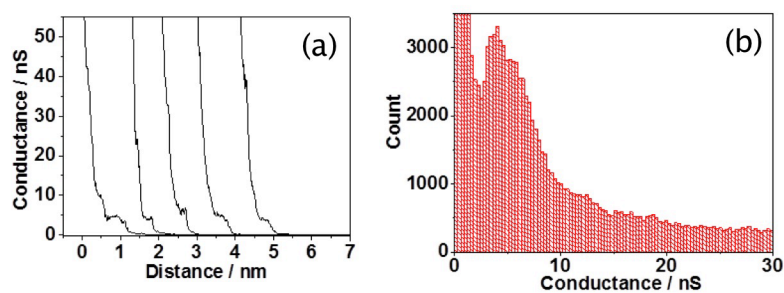


Figure S16. $I(s)$ data recorded for $[\text{Ru}(\text{MeS-ph-terpy})_2](\text{PF}_6)_2$, $I_0 = 40 \text{ nA}$, $V_{\text{bias}} = 0.6 \text{ V}$: (a) Some representative plateau(s)-containing I - s traces, (b) one-dimensional histogram of the 528 I - s traces collected that showed plateau(s).

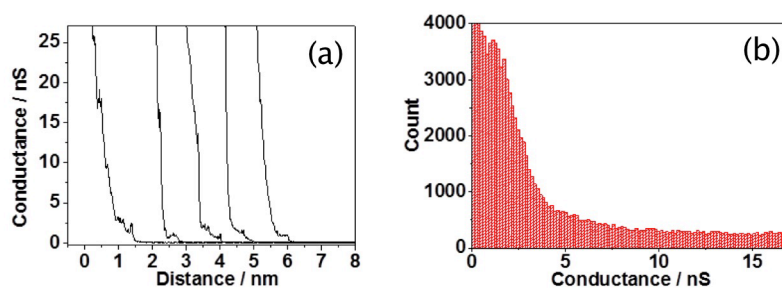


Figure S17. $I(s)$ data recorded for $[\text{Ru}(\text{MeS-ph-ph-terpy})_2](\text{PF}_6)_2$, $I_0 = 20 \text{ nA}$, $V_{\text{bias}} = 0.6 \text{ V}$: (a) Some representative plateau(s)-containing I - s traces, (b) one-dimensional histogram of the 550 I - s traces collected that showed plateau(s). In this case, the conductance was extracted from (b) using a Gaussian to fit the conductance shoulder.

3.3 $I(s)$ data from potential-dependence of conductance determinations.

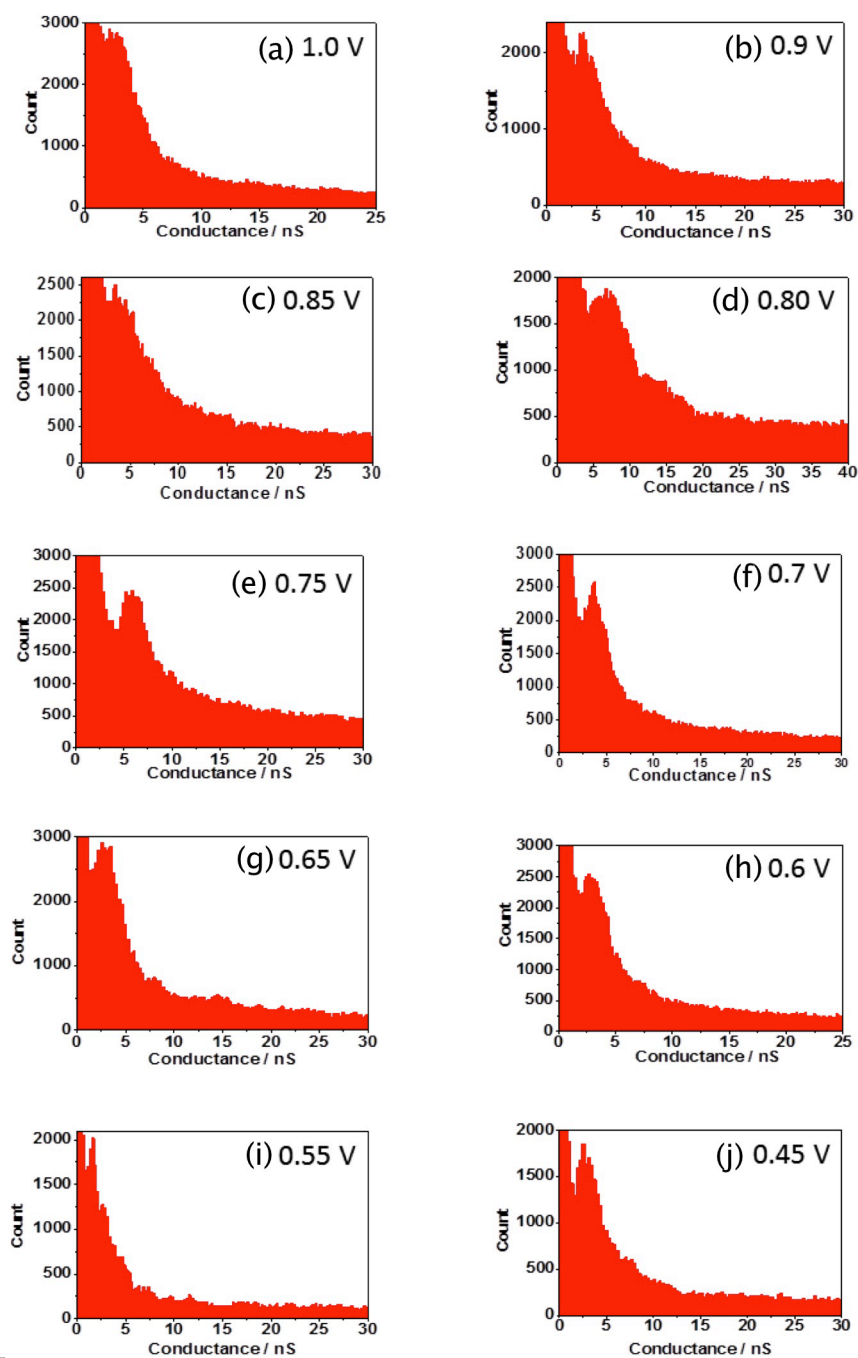


Figure S18: Conductance histograms of $[\text{Fe}(\text{pyterpy})_2](\text{PF}_6)_2$ under potential control in BMIM TFSI using sample potentials of (a) 1.00 V, (b) 0.9 V, (c) 0.85 V, (d) 0.8 V, (e) 0.75 V, (f) 0.7 V, (g) 0.65 V, (h) 0.6 V, (i) 0.55 V and (j) 0.45 V obtained using the $I(s)$ method; $V_{\text{bias}} = +0.6$ V; $I_0 = 40$ nA; 516, 502, 535, 501, 507, 501, 512, 303, 253 and 255 scans were analysed respectively. Sample potentials are with respect to the Pt quasi reference.

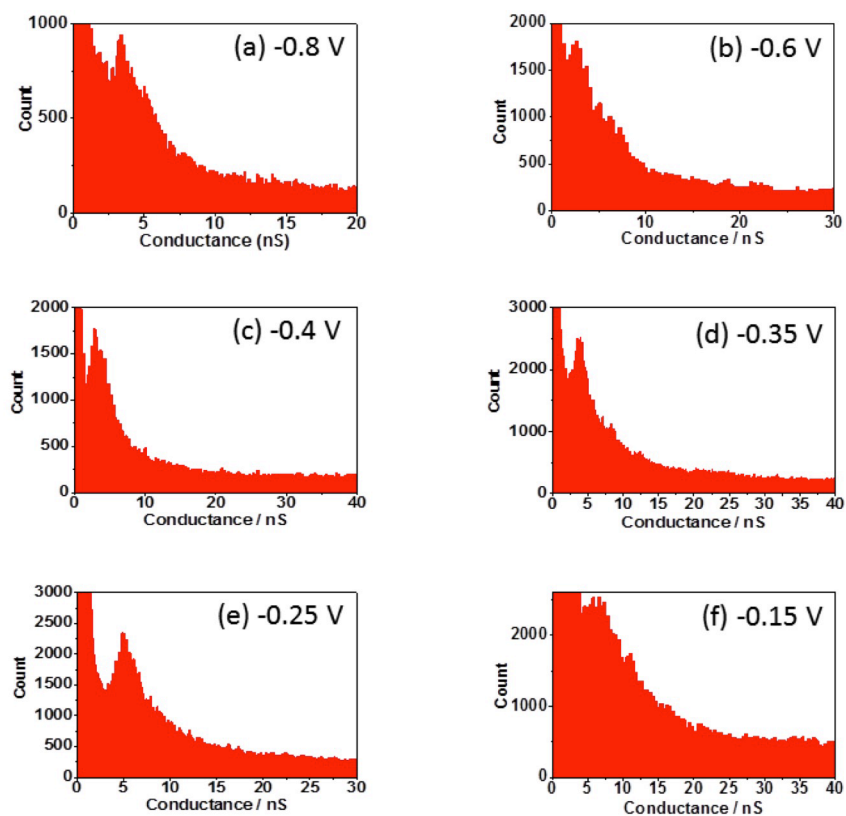


Figure S19: Conductance histograms of $[\text{Co}(\text{pyterpy})_2](\text{PF}_6)_2$ under potential control in BMIM TFSI using sample potentials of (a) -0.80 V, (b) -0.60 V, (c) -0.40 V, (d) -0.35 V, (e) -0.25 V, (f) -0.15 V obtained using the $I(s)$ method; $V_{\text{bias}} = +0.6$ V ; $I_0 = 40$ nA; 258, 309, 265, 510, 508 and 562 scans were analysed respectively. Sample potentials are with respect to the Pt quasi reference.

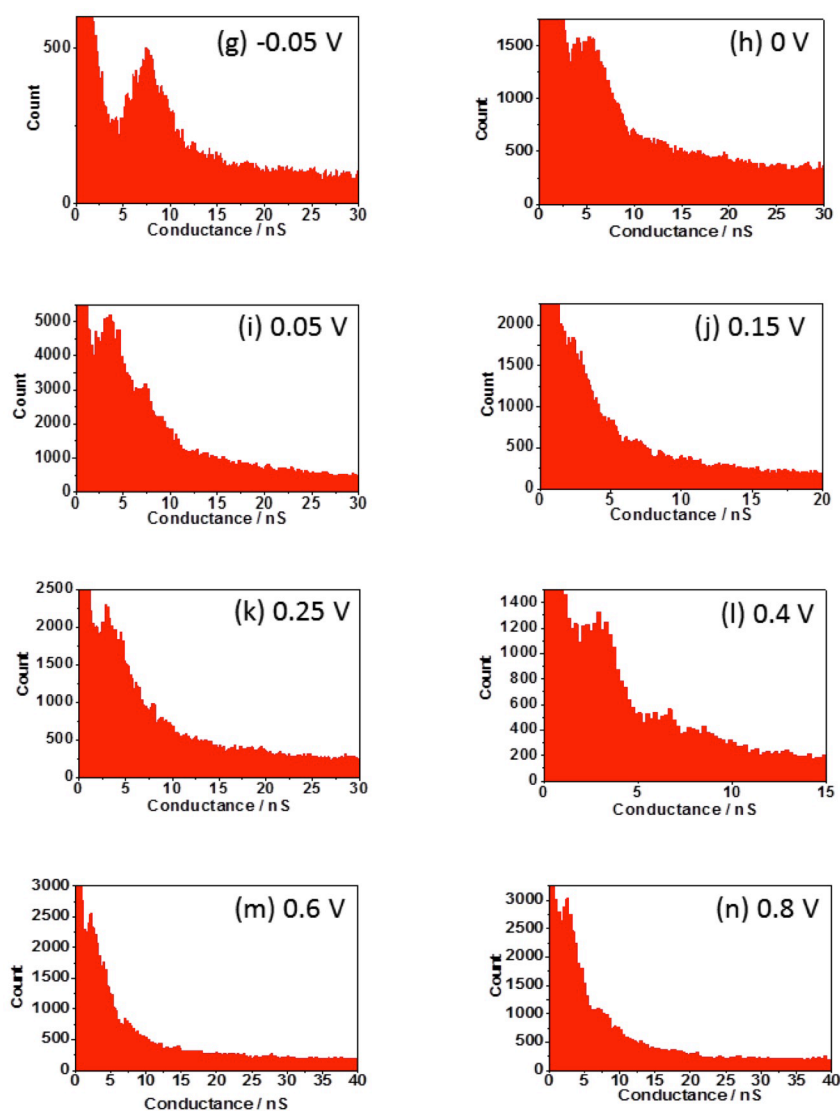


Figure S20: Further conductance histograms of $[\text{Co}(\text{pyterpy})_2](\text{PF}_6)_2$ under potential control in BMIM TFSI using sample potentials of (g) -0.05 V, (h) 0.00 V, (i) 0.05 V, (j) 0.15 V, (k) 0.25 V, (l) 0.40 V, (m) 0.60 and (n) 0.80 V respectively, obtained using the $I(s)$ method; $V_{\text{bias}} = +0.6$ V; $I_0 = 40$ nA; 491, 540, 502, 425, 421, 365, 323 and 329 scans were analysed respectively. Sample potentials are with respect to the Pt quasi reference.

4. Additional references

1. W. Haiss, D. Lackey, J. K. Sass and K. H. Besocke, *J. Chem. Phys.*, 1991, **95**, 2193-2196.
2. C. Brooke, A. Vezzoli, S. J. Higgins, L. A. Zotti, J. J. Palacios and R. J. Nichols, *Physical Review B*, 2015, **91**.
3. W. Haiss, H. van Zalinge, S. J. Higgins, D. Bethell, H. Höbenreich, D. J. Schiffrin and R. J. Nichols, *J. Am. Chem. Soc.*, 2003, **125**, 15294-15295.
4. R. J. Nichols, W. Haiss, S. J. Higgins, E. Leary, S. Martin and D. Bethell, *Physical Chemistry Chemical Physics*, 2010, **12**, 2801-2815.